Revealing multiple band structures in ^{131}Xe from α-induced reactions

R. Banik, S. Bhattacharyya, S. Biswas, Soumik Bhattacharya, G. Mukherjee, S. Rajbanshi, Shabir Dar, S. Nandi, Sajad Ali, S. Chatterjee, et al.

Revealing multiple band structures in ^{131}Xe from α-induced reaction

R. Banik,[1,2] S. Bhattacharyya,[1,2,*] S. Biswas,[3] Soumik Bhattacharya,[1,2] G. Mukherjee,[1,2] S. Rajbanshi,[4] Shabir Dar,[1,2] S. Nandi,[1,2] Sajad Ali,[5,2] S. Chatterjee,[6] S. Das,[6] S. Das Gupta,[7] S. S. Ghugre,[6] A. Goswami,[5,2,†] A. Lemasson,[3] D. Mondal,[1] S. Mukhopadhyay,[1,2] H. Pai,[5] S. Pal,[1] D. Pandit,[1] R. Raut,[6] Prithwijita Ray,[5,2] M. Rejmund,[3] and S. Samanta[6]

[1]*Variable Energy Cyclotron Centre, 1/AF Bidhannagar, Kolkata 700064, India.*
[2]*Homi Bhabha National Institute, Training School Complex, Anushaktinagar, Mumbai-400094, India.*
[3]*GANIL, CEA/DRF-CNRS/IN2P3, Bd Henri Becquerel, BP 55027, F-14076 Caen Cedex 5, France.*
[4]*Department of Physics, Presidency University, Kolkata 700073, India.*
[5]*Saha Institute of Nuclear Physics, Kolkata 700064, India.*
[6]*UGC-DAE CSR, Kolkata Centre, Kolkata 700098, India.*
[7]*Victoria Institution (College), Kolkata 700009, India.*

(Dated: March 6, 2020)

The excited states in the transitional nucleus ^{131}Xe have been populated by using α-induced fusion-evaporation reaction and the de-exciting γ rays were detected with the Compton suppressed clover detector setup of the Indian National Gamma Array (INGA) coupled to digital data acquisition system. The existing level structure of ^{131}Xe has been significantly extended with the observation and placement of 72 new γ-ray transitions. The use of light-ion (α) beam helped to identify several new band structures in ^{131}Xe with different quasi-particle (qp) configurations. The multipolarities of the observed γ rays have been determined on the basis of DCO ratio and polarization asymmetry measurements. The yrast negative parity band has been confirmed upto $35/2^-$ spin and the highly non-yrast signature partner of this band has been identified for the first time. The positive-parity band, based on the $3/2^+$ ground state, has been extended up to $23/2^+$ with the observation of a signature inversion, that signifies a pair of particle alignment around the spin of $15/2\ \hbar$. A dipole band, consisting of M1 transitions has been identified and assigned a 5-qp configuration. A new band structure built on a 3-qp $23/2^+$ state has been observed with a large signature splitting. A comparison in the isotopic and isotonic chains reveals the transitional nature of the $N = 77$ nuclei. Total Routhian surface (TRS) calculations have been performed to understand the structure of ^{131}Xe associated with different configurations.

I. INTRODUCTION

The transitional nuclei in mass 130 region, above the $Z = 50$ proton shell closure and below the $N = 82$ neutron shell closure, provide rich variety of single particle and collective structures and their coexistence [1–3]. The vibrational bands, signifying mostly the spherical structures, are more prominent in nuclei near the $N = 82$ shell closure, while the rotational bands, signifying the deformed structures, appear with several numbers of neutron holes below $N = 82$. Similar situation arises for nuclei with proton number close to or away from the $Z = 50$ shell closure. The nuclei with a few numbers of neutron holes and proton particles with respect to the $N = 82$ and $Z = 50$ shell closures are the transitional ones in this region. The structure of these transitional nuclei depends largely on the shape driving effect of the orbitals which are occupied by the odd nucleon. Most of the even-even nuclei in this transitional region are known to depict softness with respect to γ deformation [4]. It is, therefore, possible that the addition of an extra nucleon in different orbitals near the Fermi surface drives the structure of an odd-A nucleus in different shapes depending on the shape driving effect of the involved orbital. In this context, it is very interesting to study the different band structures of odd-A nuclei in the transitional region which will provide important information on the shape driving effect of different orbitals. Such effect of some of the neutron orbitals have been reported in the nuclei in $A \sim 130$ region from the observation of different rotational band structures [5, 6]. Moreover, both proton and neutron Fermi levels of the nuclei in this mass region lie within the same major shell that is $Z,\ N = 50 - 82$ shell. Hence, protons (as particles) and neutrons (as holes) can occupy different (*e.g* low-Ω and high-Ω) components of the same, high-j, $h_{11/2}$ orbital. Therefore, different polarizing effects of these components, as well as different phenomena arising due to particle-hole combination, may be manifested in the level structure of the same nucleus. This can be investigated by studying various quasiparticle (qp) excitations in nuclei of this region. The involvement of the unique-parity, high-j $h_{11/2}$ orbital plays key role in generating high spin states and is also responsible for the presence of low-lying, long-lived isomers in these nuclei with band structures built on it. Various theoretical interpretations have been applied to explain the different aspects of the level structures of nuclei in transitional region, such as, Strutinsky mean-field methods [7], Interacting Boson Model [8, 9], Pair Truncated

*Corresponding author; Electronic address: sarmi@vecc.gov.in
†Deceased

Shell Model [10], Large Scale Shell Model [11, 12] approaches, *etc.*.

The Xe ($Z = 54$) isotopes, with four proton particles beyond $Z = 50$ core and neutrons between the subshell closure $N = 64$ and the magic closed shell $N = 82$, are suitable candidates to study the various interesting features of transitional nuclei. In particular, the odd-A Xe isotopes are of interest to understand the coupling of the odd neutron to the rotational structure of the corresponding even-even core and various other possible multi-qp configurations involving valence neutrons. Odd-A Xe isotopes, with neutron number away from the $N = 82$ shell closure, have been studied up to considerable high spin demonstrating various shapes and structures. Rotational bands with large transition quadrupole moments have been observed in ^{125}Xe [13] at high spins. Recently, rotational band on a three quasineutron isomer and rotational alignment of a pair of neutron in $h_{11/2}$ have been observed in ^{127}Xe [14, 15]. The band structures in ^{129}Xe [16] have demonstrated triaxial shapes. On the other hand, a dipole band, observed at high spin in the $N = 69$ isotope ^{123}Xe [17], was proposed to have an intermediate character of Magnetic Rotation (MR) and collective rotation, which could be explained by tilted axis configuration involving $h_{11/2}$ proton particles and $h_{11/2}$ neutron holes. As the neutron Fermi surface increases, such MR bands are expected to be more favourable as the high-Ω components of the $h_{11/2}$ orbital are energetically more accessible to the odd-neutrons. However, such bands could not be seen in ^{125,129}Xe. This could be either due to the fact that the particular configuration for which MR bands are expected have not been populated or because the shapes of these nuclei are not near spherical, which is a required condition for an MR band to observe. For even heavier isotopes of Xe, close to the $N = 82$, though near-spherical shapes are expected, the high spin spectroscopic information is very limited. Therefore, in order to understand the various coupling schemes and to investigate the systematics of the different multi-quasiparticle configurations in the Xe isotopes of transitional region, it is necessary to have detailed spectroscopic information of both yrast and non-yrast states involving multi-qp excitations in the heavier Xe isotopes. It is, however, difficult to populate the excited states up to very high spin in the higher mass Xe isotopes with the available stable target and heavy-ion projectile combinations. Therefore, we have employed light-ion (α) induced reaction to populate the excited states in ^{131}Xe to investigate its excited states.

The level structures of ^{131}Xe was first studied using offline decay spectroscopy technique [18, 19] and Coulomb excitation measurements [20]. These results are mostly limited to the low-spin levels. Angular correlation measurements were also performed for a few states of ^{131}Xe in Ref. [21] to assign the spin and parity of some of these states. The in-beam measurements of the high spin states of ^{131}Xe, were first carried out using (α, 3n) [22] and (α, n) [3] reactions with a few Ge(Li) detectors, where, one- and three-qp states at low spins were unambiguously identified. Detailed spectroscopic information could not be obtained in these studies, mainly due to the limitation in the detection system. Recently, excited states in ^{131}Xe at higher spins have been reported by Kaya *et.al* [12], using two independent reactions, namely, multinucleon transfer reaction involving ^{136}Xe beam and ^{124}Sn(^{11}B, $p3n$) fusion-evaporation reaction. The yrast negative parity band, built on the $11/2^-$ isomer in ^{131}Xe was extended in this work up to 4.9 MeV of excitation and up to tentatively assigned spin of $35/2\ \hbar$, with the placement of three new γ transitions. No other band structures could be identified in this work. The spin and parity of some of the states were also could not be firmly assigned due to the lack of statistics.

In the present work, the yrast and non-yrast structures of ^{131}Xe have been investigated using α-induced fusion-evaporation reaction. The large cross section ($\sim$ 1 b) of the three-neutron evaporation channel of α-induced fusion reaction allows us to carry out a detailed spectroscopy of various band structures of ^{131}Xe. Moreover, α induced reactions can have considerable feeding to both the yrast and the non-yrast states, which can be investigated in detail with the help of a high resolution γ detector array. The present work reports new results of yrast and various non-yrast band structures in ^{131}Xe involving different single- and multi-qp excitations. The quasi-particle configurations, modes of excitation and the structures associated with these bands have been investigated and compared with the other isotopes and isotones.

II. EXPERIMENT

In the present study, the excited states of ^{131}Xe have been populated via the reaction ^{130}Te(α, $3n$)^{131}Xe at a beam energy of 38 MeV obtained from the K-130 cyclotron at Variable Energy Cyclotron Centre, Kolkata (India). At this beam energy, the production cross section of ^{131}Xe has been estimated to be $\sim 90\%$ of the total fusion evaporation reaction cross section. An enriched ^{130}Te target of thickness 2 mg/cm^2, evaporated on a 600 μg/cm^2 Mylar backing, was used for the present experiment. The Indian National Gamma Array (INGA) setup at VECC [23], Kolkata, consisting of seven Compton suppressed clover HPGe detectors was used for detecting the emitted γ-rays from the produced nuclei. Four clover HPGe detectors were placed at an angle of 90°, two detectors were at backward 55° and one detector was at forward 40° with respect to the beam direction. The clover detectors were placed at a distance of 25 *cm* from the target position. The pulse processing and data acquisition system of the INGA setup was based on PIXIE-16 250 MHz 12-bit digitizer modules [24]. Time stamped list mode data was acquired under the event trigger condition based on Compton suppressed clover detector multiplicity (M_γ), set either in coincidence ($M_\gamma \geq 2$) or in singles ($M_\gamma \geq 1$) mode. Standard ^{133}Ba and ^{152}Eu radioactive

sources, placed at the target position were used for energy and efficiency calibration of the setup.

III. DATA ANALYSIS

The data were sorted using the IUCPIX [24] data sorting package to gain match the data from all the four crystals and then generate the addback spectra of each clover detector, after ensuring Compton suppression by vetoing the corresponding BGO shield. These addback data were then used to construct the symmetric and angle dependent asymmetric E_γ-E_γ matrices and the E_γ-E_γ-E_γ cube. The RADWARE [25] and LAMPS [26] analysis packages were then used to analyze these matrices and the cube, to obtain various coincidence relationships between the decaying γ-transitions and to determine their multipolarities and subsequently construct the level scheme. Fig. 1 shows the one dimensional projection of the symmetric E_γ-E_γ matrix, as obtained in the present work. In this figure, the marked γ-rays are mostly from ^{131}Xe, which indicates that the α-induced reaction dominantly produces a single channel with large cross-section.

An asymmetric matrix was also constructed in order to obtain the ratio of Directional Correlation from Oriented states (R_{DCO}) [27] which was used to extract the information on the multipolarity of a given γ-ray. The data from the 90° (θ_1) detectors and from the backward 55° (θ_2) detectors were put at the X and Y axes of this asymmetric matrix, respectively. The R_{DCO} of a γ transition (γ_1) is defined as the ratio of its intensities (I_γ) at the two different angles θ_1 and θ_2, gated by another stretched transition (γ_2) of known multipolarity, as per the following expression:

$$R_{DCO} = \frac{I_{\gamma_1} \text{at } \theta_1, \text{ gated by } \gamma_2 \text{ at } \theta_2}{I_{\gamma_1} \text{at } \theta_2, \text{ gated by } \gamma_2 \text{ at } \theta_1} \qquad (1)$$

In the present analysis, the R_{DCO} was found to be close to 1.0 for a pure stretched quadrupole or dipole transition, when gated by a stretched transition of same multipolarity. When the gating transition is of different multipolarity, the R_{DCO} was found to be ~ 0.6 (1.9) for a stretched dipole (quadrupole) transition, when gated by a stretched quadrupole (dipole) transition.

Polarization asymmetry measurements of the decaying γ-transitions were carried out to assign the parities to the excited levels. The measurement of the Polarization Directional Correlation asymmetry parameter (Δ_{PDCO}) of the decaying γ-rays, as described in the Ref. [28, 29], were used to deduce the electric or magnetic nature of the γ-rays. Four clover detectors, placed at 90° in the setup, were used for the Δ_{PDCO} measurements. The Δ_{PDCO} is defined as,

$$\Delta_{PDCO} = \frac{a(E_\gamma)N_\perp - N_\parallel}{a(E_\gamma)N_\perp + N_\parallel} \qquad (2)$$

where, $N_\parallel$ and $N_\perp$ represents the counts corresponding to the Compton scattered events of a γ-ray in parallel and perpendicular direction with respect to the reaction plane, respectively. $a(E_\gamma)$, which is defined as $a(E_\gamma)$=$N_\parallel/N_\perp$, is the geometrical asymmetry correction factor of the detection setup. The factor $a(E_\gamma)$ can be obtained from the Compton scattered events of the γ rays from an unpolarized source. In the present work, the decay transitions from ^{152}Eu standard radioactive source were used to extract the value of $a(E_\gamma)$ from the fitting of its variation as a function of γ-ray energy (E_γ), using the equation $a(E_\gamma) = a_0 + a_1 E_\gamma$. The values of the coefficients are obtained as $a_0 = 1.003(5)$ and $a_1 = 1.92(1) \times 10^{-6}$. Fig. 2 shows the variation of the asymmetry factor ($a(E_\gamma)$) as a function of incident γ-ray energy (E_γ), for the present setup. In order to obtain the Δ_{PDCO} of a γ ray, its parallel and perpendicular scattered components were extracted from the two asymmetric matrices, having parallel and perpendicular scattered events of the 90° clover detectors along Y-axis and events from all the other detectors along the X-axis. The positive and negative values of the Δ_{PDCO} correspond to the electric and magnetic nature of the transition respectively.

IV. RESULTS

The level scheme of ^{131}Xe, obtained from current measurements is shown in Fig. 3. The level structure is significantly extended, compared to the previous studies [12, 22], with the placement of 72 new γ-rays in the level scheme of ^{131}Xe. It is evident from Fig. 3 that the level structure has been expanded with the observation of several yrast and near yrast states above the $11/2^-$ isomer (11.84 days) at 164 keV excitation, as well as above the $3/2^+$ ground state. It is possible to access such states upto the medium spin regime because of the use of light ion induced reaction. The various sequences of γ rays in the level scheme are marked as $B1$ to $B6$ for the convenience of describing them. The spin-parities of most of these states could be assigned from the deduced DCO ratio (R_{DCO}) and polarization asymmetry (Δ_{PDCO}). The R_{DCO} and Δ_{PDCO} values of the new transitions identified from the present work, along with some of the representative known transitions of energies 444, 642 and 795 keV, are plotted as a function of γ ray energy in Fig. 4(a) and 4(b), respectively. The intensities of the observed γ rays are determined from the various relevant coincidence spectra and subsequently normalized to the intensity of the strongest 642 keV transition above $11/2^-$ isomer. The energies of the observed γ rays along with the corresponding level energies, relative intensities, R_{DCO}, Δ_{PDCO} and the assigned multipolarities are tabulated in Table I. The γ rays with the R_{DCO} values in the range of 0.5 to 0.7 obtained in a quadrupole gate and 0.9 to 1.1 in a dipole gate with negative Δ_{PDCO} values, are considered as dominantly M1 with possible small E2 admixture and are mentioned as M1(+E2) in Table I.

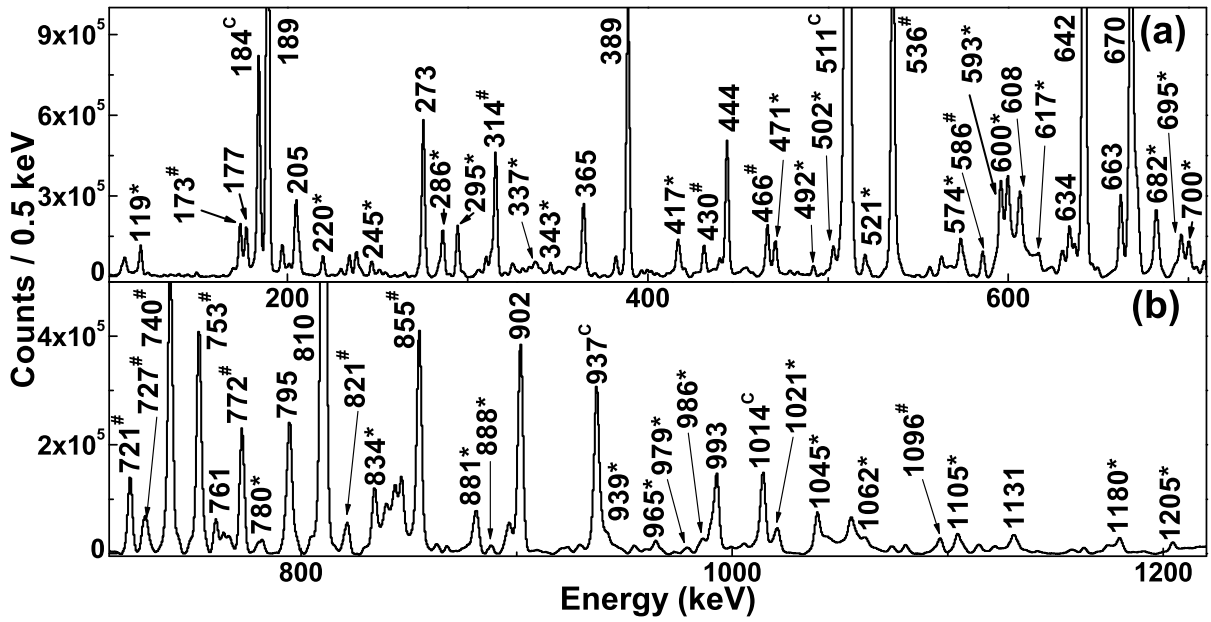

FIG. 1: Total projection of the E_γ-E_γ matrix. Energy of the observed γ-rays of are marked. The new transitions of ^{131}Xe, identified from the present work, are marked with $*$. Energy upto 710 keV is shown in (a) and above 710 keV is shown in (b).The transitions of neighbouring channel produced in the same reaction are marked as '#' and the γ-rays marked with 'c' are the contaminant γ rays from reactions with Mylar backing and Al frame.

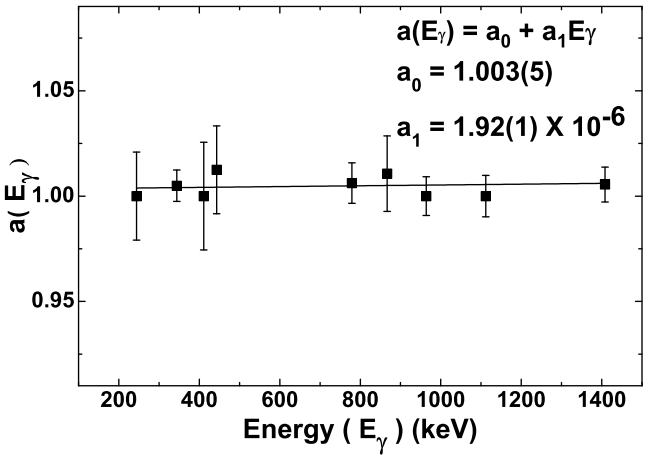

FIG. 2: Variation of the asymmetry parameter $a(E_\gamma)$ as a function of incident γ-ray energy (E_γ), as obtained for the present experimental set up, using standard unpolarised radioactive sources. The linear fitting of $a(E_\gamma)$ as a function of γ ray energy (E_γ) is also shown.

Whereas, the γ rays with the R_{DCO} values outside the above range and with negative Δ_{PDCO} values are considered to be of mixed nature and mentioned as M1+E2.

From the earlier studies on ^{131}Xe, using (α, 3n) reaction [22], only few states above the $11/2^-$ isomer were reported with the observation of 642, 810, 902 keV transitions of the main yrast sequence and 795, 205, 189, 444, 389, 993 keV transitions connecting to the yrast sequence. The yrast negative parity band $B1$ has been extended recently by Kaya *et al.* [12] with the observation of three transitions of energy 663, 634 and 1131 keV assigned to this sequence. In the present work, several other new sequences of γ rays could be identified as decaying from near yrast states and connecting to the yrast band $B1$. Also, well developed structures of $B3$ and $B4$ have been observed, compared to the previous studies. Fig. 5(a)-(c) shows the coincidence spectra corresponding to the γ ray gates of 902, 189 and 397 keV respectively. The development of three separate parallel branches above the 1617 keV level is evident from the observation of different set of γ rays in coincidence with the 902, 189 and 397 keV transitions. It can also be seen from Fig. 5(a) that, other than three transitions of 663, 634 and 1131 keV, reported by Kaya *et al.* [12], various new transitions are observed in coincidence with the 902 keV. Similarly, in the coincidence gate of 189 keV (Fig. 5(b)), except the 389, 444 and 993 keV γ rays, reported by Kerek *et al.* [22], all the other γ rays are new and observed first time from the present work. The coincidence spectrum of 397 keV gate, as shown in Fig. 5(c), establishes the new sequence $B2$ consisting of three transitions of 397, 593 and 979 keV, in cascade.

Band $B1$ is the negative parity yrast band which is observed upto an excitation of 4945 keV and spin of $35/2\ \hbar$. The top three transitions of this band have also been reported recently by Kaya *et al.* [12], but the spin-parity of the 3815 and 4945 keV levels could only be assigned tentatively. From the present work, the spin assignments

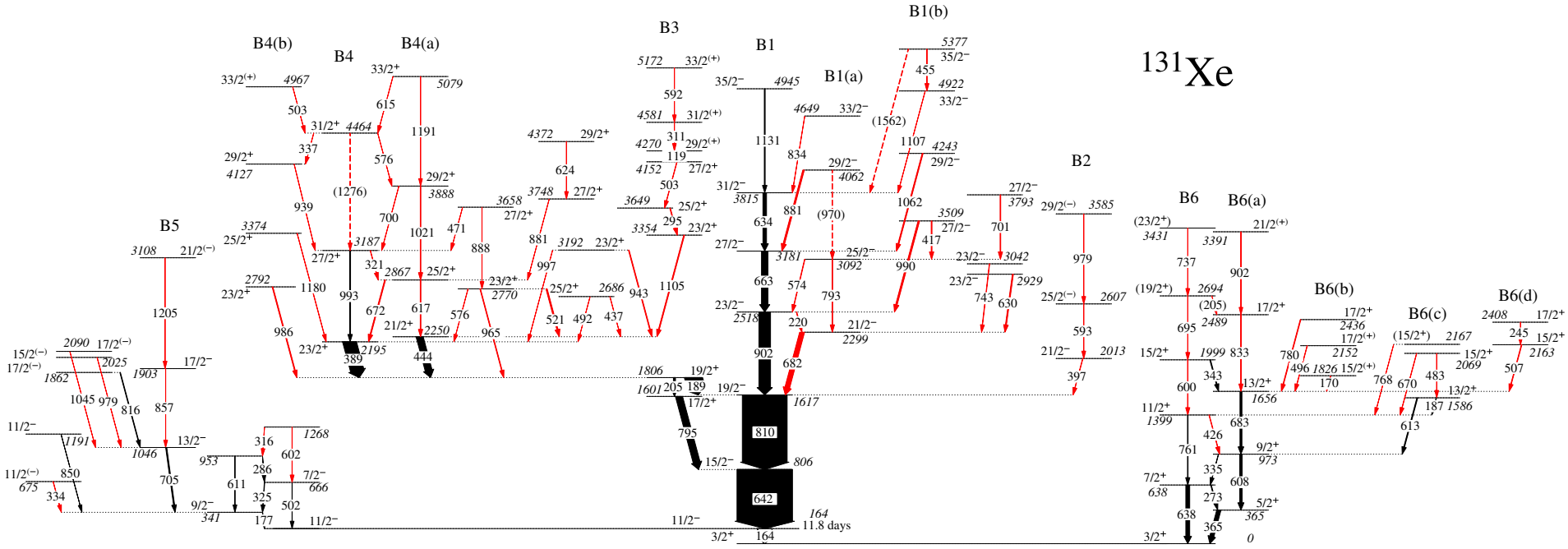

FIG. 3: Proposed level scheme of ^{131}Xe, as obtained from the present work. The new γ rays observed are marked in red.

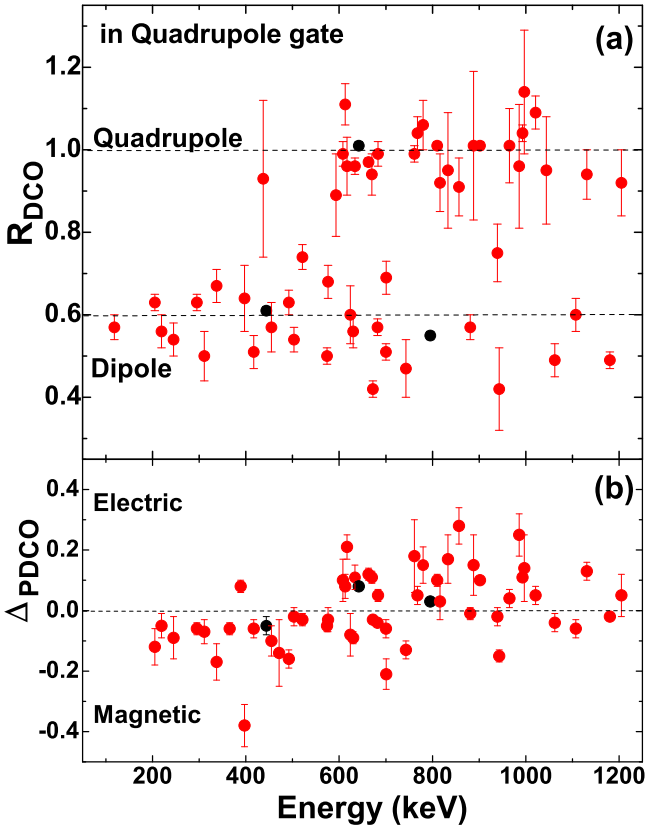

FIG. 4: (a) The DCO ratio (R_{DCO}) and (b) the polarization asymmetry (Δ_{PDCO}) of the new γ rays (in red), and those of the known γ rays of energy 444 (M1), 642 (E2) and 795 (E1) keV (in black), as obtained in the present work, are plotted as a function of γ ray energy. The R_{DCO} values shown in the plot are obtained in quadrupole gates only. The dotted lines at Y-axis in (a) are to guide the eye for the DCO ratio corresponding to pure dipole and quadrupole transitions respectively. The dotted line at Y-axis in (b) is to guide the eye for Δ_{PDCO} values corresponding to the electric (+ve) and magnetic (-ve) nature of the transitions.

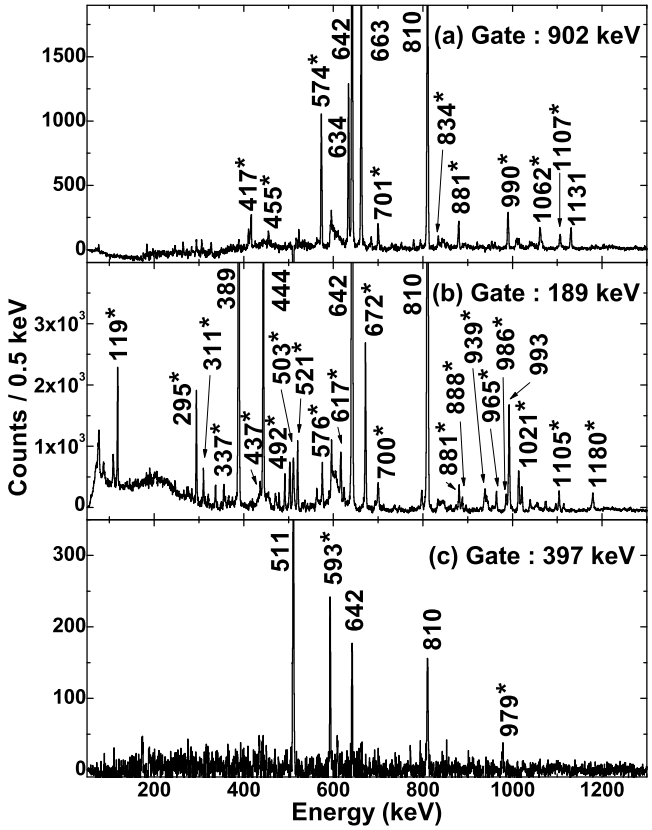

FIG. 5: Coincidence spectra corresponding to the γ ray gates of (a) 902 keV of band $B1$, (b) 189 keV connecting to band $B1$ and (c) 397 keV of band $B2$ from E_γ-E_γ matrix. The new transitions observed in the present work are marked with $*$.

of these two states are confirmed as $31/2^-$ and $35/2^-$ respectively, from the R_{DCO} and Δ_{PDCO} measurements. The deduced E2 character of the 902 keV transition of this band from the present measurements, also supports the assignment by Kaya *et al.* [12], which was earlier reported as M1 in Ref. [22]. Fig. 6(a) shows the double gate of the 642 and 902 keV transitions of the yrast band $B1$, which shows the transitions related to the band $B1$. It can be seen that, other than the transitions of main yrast sequence $B1$, there are several new transitions in coincidence with the 642-902 cascade. From the present work, a possible signature partner of the yrast band $B1$ can be established with the observation of a parallel sequence of levels, marked as $B1$(a) in Fig. 3. These levels are connected to the 1617, 2518, 3181 and 3815 keV levels of $B1$ by M1 transitions. The presence of $B1$(a) is evident from Fig. 6(b)-(c), which show the coincidence spectra corresponding to the double gates of the 642 & 663 keV and 642 & 682 keV respectively. Comparing Fig. 6(a) and Fig. 6(b), it is clear that the 574, 990, 701 and 417 keV transitions are in coincidence with 902 keV, but in parallel to 663 keV transition. On the other hand, comparing Fig. 6(a) and Fig. 6(c), it is clear that the set of new transitions of energies 220, 630, 743 and 793 keV are in coincidence with the 642-810-682 keV cascade, but not with the 642-810-902 keV cascade. Thus the 682 keV transition is connected to a separate branch, in parallel to the 902 keV transition. The presence of a strong 220 keV transition in coincidence with the 682 keV places the 682-220 keV cascade in parallel to the 902 keV transition. The M1 nature of the connecting transitions between $B1$ and $B1$(a) have been established from the measured R_{DCO} and Δ_{PDCO} values, given in Table I. The placement of the γ rays in $B1$, $B1$(a) and $B1$(b) in the level scheme of ^{131}Xe (Fig. 3) is also supported by the coincidence spectra of the 663 and 634 keV, as shown in Fig. 7(a) and Fig. 7(b), respectively. The 1062 and 881 keV transitions are placed above the 3181 keV level as they are in coincidence with the 663 keV transition, but not with the 634 keV, as seen from Fig. 7(a) and 7(b). It can also be seen from these coincidence spectra that the 1107-455 keV cascade is in

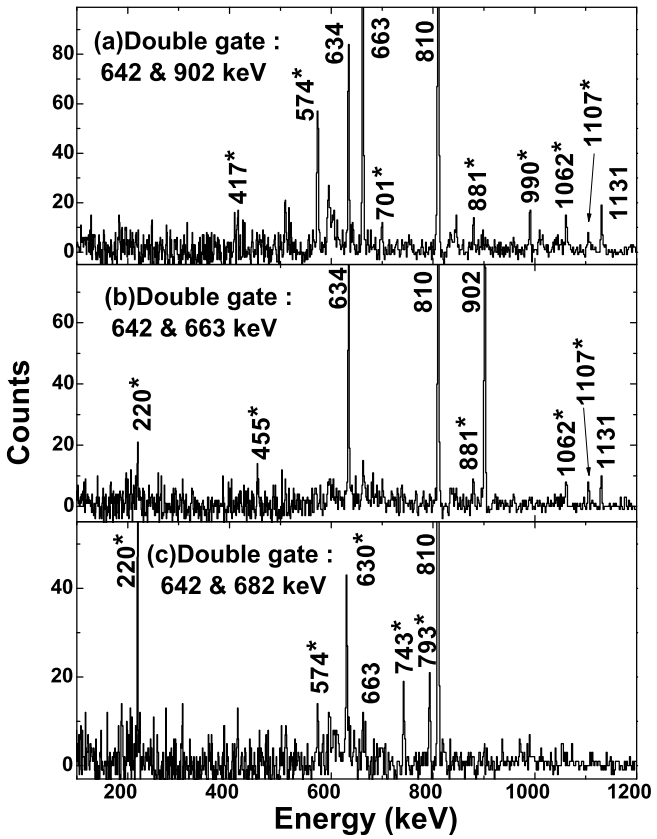

FIG. 6: Coincidence spectra corresponding to the double gates of (a) 642 & 902 keV, (b) 642 & 663 keV and (c) 642 & 682 keV transitions of band $B1$from E_γ-E_γ-E_γ cube. The new transitions observed in the present work are marked with $*$.

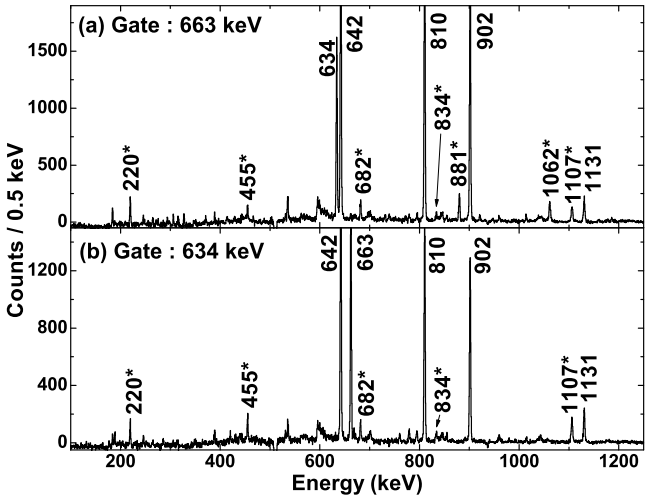

FIG. 7: Coincidence spectra corresponding to the gates of (a) 663 keV and (b) 634 keV transitions of band $B1$ obtained from E_γ-E_γ matrix. The new transitions observed in the present work are marked with $*$.

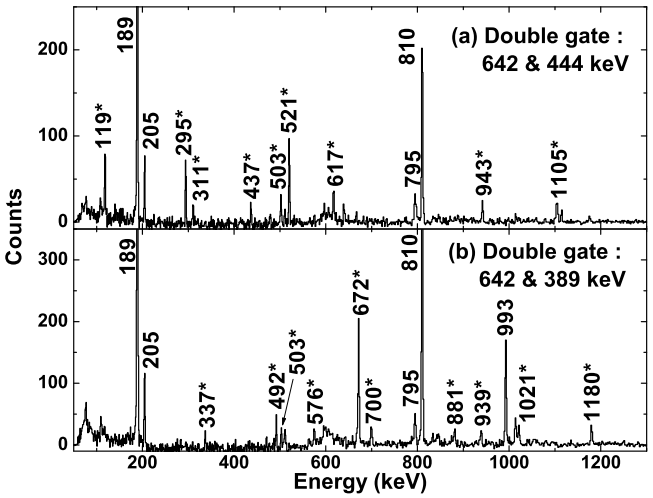

FIG. 8: Coincidence spectra corresponding to the double gates of (a) 642 & 444 keV and (b) 642 & 389 keV transitions from E_γ-E_γ-E_γ cube. The new transitions observed in the present work are marked with $*$.

coincidence with both 663 and 634 keV transitions and therefore placed above the 3815 keV level.

Above the 1806 keV level having spin $19/2^+$, there are two parallel branches developed, marked as $B3$ and $B4$ (divided into bands $B4$, $B4$(a) and $B4$(b)) in the level scheme (Fig. 3). One of them is in coincidence with the 444 keV M1 transition and another is in coincidence with the 389 keV E2 transition. The 1806 keV level having spin $19/2^+$ decays to the 806 keV level having spin $15/2^-$ of band $B1$ via the 205-795 keV cascade and to the 1617 keV level having spin $19/2^-$ of band $B1$ via the 189 keV transition. Among these two decay paths, the 189 keV transition is more intense in comparison to the 205-795 keV cascade. The coincidence spectra corresponding to the double gates of the 642 & 444 keV and 642 & 389 keV are shown in Fig. 8(a) and (b), respectively. It can be clearly seen from this figures, that two completely different set of γ rays are present connected to the 444 keV and 389 keV transitions.

The sequence $B3$ consists of M1 γ-transitions above the 2250 keV level having spin $21/2^+$ and is extended upto the 5172 keV level with spin $33/2^{(+)}$). From the current work, 1105, 295, 503, 119, 311 and 592 keV transitions have been placed above the 2250 keV level, in coincidence with the 444 keV transition, which is evident from Fig. 8(a). The placement of these transitions are done on the basis of their relative intensities. The multipolarities of these transitions were determined from the R_{DCO} values, obtained from the gates of 795 keV E1 transition and 810 keV E2 transition. Along with this, the deduced negative Δ_{PDCO} for these transitions make them as of M1 character. As the 119 keV low energy transition did not have enough Compton scattering, so its polarization asymmetry (Δ_{PDCO}) could not be determined. However, the dipole nature of this transition could be confirmed from the deduced R_{DCO} value

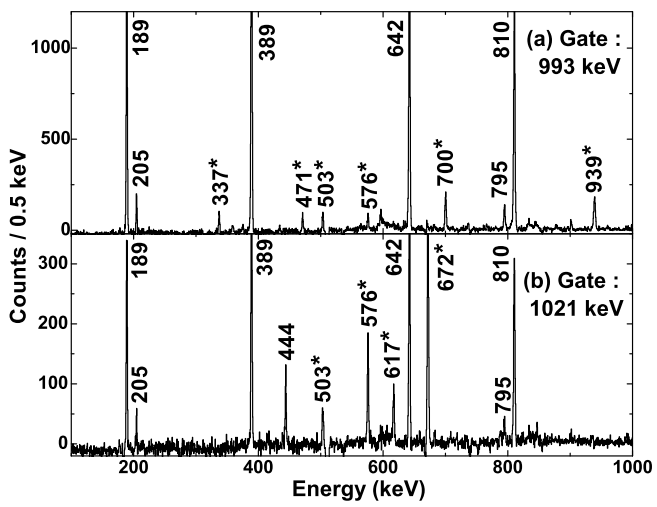

FIG. 9: Coincidence spectra corresponding to the gates of (a) 993 keV of band $B4$ and (b) 1021 keV of band $B4$(a), obtained from the E_γ-E_γ matrix. The new transitions observed in the present work are marked with $*$.

of 0.57(3) in the quadrupole gate of 810 keV. Thus, the parity of the 4270 keV level, depopulated by the 119 keV and hence the parities of the levels above it have been assigned only tentatively.

The bands $B4$ and $B4$(a) are built on the 2195 keV level with spin $23/2^+$ and consists of a sequence of five M1 transitions of energies 672, 321, 700, 576 and 615 keV. The corresponding levels are also connected by the E2 crossover transitions. From the present work, the bands $B4$-$B4$(a) has been established upto 5079 keV excitation. Another sequence of levels have been found at 3374, 4127 and 4967 keV with spins $25/2^+$, $29/2^+$ and $33/2^{(+)}$, respectively. These states, named as $B4$(b), are connected to the states of band $B4$ via ΔJ=1 transitions. But no connection of E2 transitions in between these levels could be observed. The new transitions of this band and their placements have been established from the various coincidence relationships found from the E_γ-E_γ matrix. The coincidence spectra of the 993 and 1021 keV γ ray gates are shown in Fig. 9(a) and (b) respectively. It can be seen from this figure, that the 337, 471, 700 and 939 keV transitions are in coincidence with the 993 keV, but not with the 1021 keV and placed accordingly. Whereas, the 672 keV transition is in coincidence with the 1021 keV but not with the 993 keV, thus placed parallel to the 993 keV transition. The other two levels at 2770 and 3658 keV are found to decay to the band $B4$ by non-stretched transitions of energies 576 and 471 keV respectively. The multipolarities of the transitions of band $B4$, $B4$(a) and $B4$(b) have been found from the R_{DCO} values extracted from the gate of 389 keV stretched quadrupole transition.

TABLE I: The energies (E_γ) and relative intensities (I_γ) of the γ rays observed in ^{131}Xe along with the spin and parity of the initial (J_i^π) and the final (J_f^π) states and the energy of the initial state (E_i). The level energies (E_i) are obtained by least-squares fitting to the γ-ray energies (E_γ) using GTOL [30]. The measured values of R_{DCO} and Δ_{PDCO} are also shown along with the proposed multipolarity of the γ rays.

E_γ(Err) (in keV)	E_i(Err) (in keV)	$J_i^\pi \rightarrow J_f^\pi$	I_γ(Err) [1]	R_{DCO}(Err)	Δ_{PDCO}(Err)	Deduced Multipolarity
118.5(1)	4270.1(4)	$29/2^{(+)} \rightarrow 27/2^+$	0.37(3)	0.57(3)[2]	-	(M1+E2)
170.3(1)	1826.3(2)	$15/2^{(+)} \rightarrow 13/2^+$	0.15(6)	0.59(9)[3]	-	(M1+E2)
177.1(1)	341.2(2)	$9/2^- \rightarrow 11/2^-$	3.36(17)	0.57(2)[4]	-	(M1+E2)[14]
186.6(1)	1585.9(1)	$13/2^+ \rightarrow 11/2^+$	0.11(2)	-	-	(M1+E2)
188.8(1)	1805.6(3)	$19/2^+ \rightarrow 19/2^-$	31(2)	0.82(2)[5]	0.11(3)	E1
204.8(1)	1805.6(3)	$19/2^+ \rightarrow 17/2^+$	3.24(16)	0.63(2)[5]	-0.12(6)	M1(+E2)
204.8(1)	2693.9(2)	$(19/2^+) \rightarrow 17/2^+$	-	-	-	(M1+E2)
219.5(1)	2518.4(3)	$23/2^- \rightarrow 21/2^-$	0.86(5)	0.56(4)[5]	-0.05(4)	M1(+E2)
244.7(1)	2407.8(2)	$17/2^+ \rightarrow 15/2^+$	0.22(8)	0.54(4)[6]	-0.09(7)	M1(+E2)
273.2(1)	637.9(1)	$7/2^+ \rightarrow 5/2^+$	1.07(6)	0.86(9)[6]	-	(M1+E2)
286.3(1)	952.6(2)	$\rightarrow 7/2^-$	0.08(1)	-	-	-
294.5(1)	3648.8(3)	$25/2^+ \rightarrow 23/2^+$	1.09(9)	0.63(2)[2]	-0.06(2)	M1(+E2)
310.6(1)	4580.7(4)	$31/2^{(+)} \rightarrow 29/2^{(+)}$	0.22(2)	0.50(6)[2]	-0.07(4)	M1(+E2)
315.5(1)	1268.1(2)		0.07(1)	-	-	-
320.8(1)	3187.3(3)	$27/2^+ \rightarrow 25/2^+$	0.08(1)	0.68(10)[7]	-	(M1+E2)
325.2(1)	666.4(2)	$7/2^- \rightarrow 9/2^-$	0.67(3)	1.21(5)[8]	-0.03(2)	M1+E2
334.2(1)	675.4(2)	$11/2^{(-)} \rightarrow 9/2^-$	0.55(3)	1.08(7)[8]	-	(M1+E2)
334.9(1)	972.8(1)	$9/2^+ \rightarrow 7/2^+$	0.48(4)	0.55(3)[9]	-	(M1+E2)
337.0(1)	4463.6(3)	$31/2^+ \rightarrow 29/2^+$	0.11(1)	0.67(4)[7]	-0.17(6)	M1(+E2)
342.5(1)	1998.7(1)	$15/2^+ \rightarrow 13/2^+$	1.34(15)	0.76(5)[3]	-0.18(9)	M1+E2
364.8(1)	364.7(1)	$5/2^+ \rightarrow 3/2^+$	7.30(91)	0.69(3)[6]	-0.06(2)	M1(+E2)
389.0(1)	2194.6(3)	$23/2^+ \rightarrow 19/2^+$	24(1)	1.09(2)[5]	0.08(2)	E2

Table I: Continued...

E_γ(Err) (in keV)	E_i(Err) (in keV)	$J_i^\pi \rightarrow J_f^\pi$	I_γ(Err) [1]	R_{DCO}(Err)	Δ_{PDCO}(Err)	Deduced Multipolarity
396.6(1)	2013.3(3)	$21/2^- \rightarrow 19/2^-$	0.88(4)	0.64(8)[5]	-0.18(7)	M1(+E2)
416.8(1)	3508.8(3)	$27/2^- \rightarrow 25/2^-$	1.35(8)	0.51(4)[5]	-0.06(3)	M1(+E2)
426.4(1)	1399.1(1)	$11/2^+ \rightarrow 9/2^+$	0.71(6)	-	-	(M1+E2)
436.8(1)	2686.4(3)	$25/2^+ \rightarrow 21/2^+$	0.37(3)	0.93(19)[2]	-	(E2)
444.0(1)	2249.5(3)	$21/2^+ \rightarrow 19/2^+$	12.42(62)	0.61(1)[5]	-0.05(3)	M1(+E2)
454.8(2)	5376.6(3)	$35/2^- \rightarrow 33/2^-$	0.52(4)	0.57(6)[10]	-0.10(5)	M1(+E2)
470.8(1)	3658.1(3)	$27/2^+ \rightarrow 27/2^+$	0.08(1)	0.71(9)[7]	-0.14(11)	M1+E2
483.0(1)	2069.0(1)	$15/2^+ \rightarrow 13/2^+$	1.66(14)	0.71(16)[3]	-0.09(6)	M1+E2
492.0(1)	2686.4(3)	$25/2^+ \rightarrow 23/2^+$	0.19(3)	0.63(3)[7]	-0.16(3)	M1(+E2)
496.4(1)	2152.4(2)	$17/2^{(+)} \rightarrow 13/2^+$	0.55(7)	1.01(13)[6]	-	(E2)
502.4(1)	666.4(2)	$7/2^- \rightarrow 11/2^-$	2.81(31)	-	-	(E2)[14]
502.8(1)	4151.6(3)	$27/2^+ \rightarrow 25/2^+$	0.58(5)	1.09(17)[11]	-0.15(4)	M1(+E2)
503.2(1)	4966.8(3)	$33/2^{(+)} \rightarrow 31/2^+$	0.19(1)	0.54(3)[7]	-0.02(3)	M1+E2
507.1(1)	2163.1(2)	$15/2^+ \rightarrow 13/2^+$	0.32(4)	0.71(8)[6]	-0.10(3)	M1+E2
520.9(2)	2770.3(3)	$23/2^+ \rightarrow 21/2^+$	2.23(18)	0.74(3)[2]	-0.03(2)	M1+E2
573.6(2)	3092.0(3)	$25/2^- \rightarrow 23/2^-$	0.77(13)	0.50(2)[5]	-0.05(2)	M1(+E2)
575.8(1)	2770.3(3)	$23/2^+ \rightarrow 23/2^+$	0.27(3)	0.68(4)[7]	-0.01(2)	M1+E2
575.9(1)	4463.6(3)	$31/2^+ \rightarrow 29/2^+$	0.10(2)	0.63(4)[12]	-0.03(4)	M1+E2
591.5(1)	5172.2(4)	$33/2^{(+)} \rightarrow 31/2^{(+)}$	0.22(2)	1.05(17)[11]	-	(M1+E2)
593.3(1)	2606.6(3)	$25/2^{(-)} \rightarrow 21/2^-$	0.48(10)	0.89(10)[5]	-	(E2)
599.7(1)	1998.7(1)	$15/2^+ \rightarrow 11/2^+$	0.81(10)	0.96(8)[9]	0.08(7)	E2
601.7(1)	1268.1(2)	$\rightarrow 7/2^-$	0.42(8)	-	-	-
608.3(1)	972.8(1)	$9/2^+ \rightarrow 5/2^+$	4.82(22)	0.99(3)[6]	0.10(7)	E2
611.4(1)	952.6(2)	$\rightarrow 9/2^-$	0.34(3)	-	-	-
613.1(1)	1585.9(1)	$13/2^+ \rightarrow 9/2^+$	1.79(31)	1.11(5)[3]	0.08(4)	E2
615.1(1)	5078.7(3)	$33/2^+ \rightarrow 31/2^+$	0.06(4)	-	-	(M1+E2)
617.2(1)	2866.5(3)	$25/2^+ \rightarrow 21/2^+$	1.09(9)	0.96(7)[2]	0.21(4)	E2
624.1(1)	4371.8(3)	$29/2^+ \rightarrow 27/2^+$	0.07(2)	0.60(7)[7]	-0.08(7)	M1(+E2)
630.2(2)	2929.2(4)	$23/2^- \rightarrow 21/2^-$	1.83(11)	0.56(4)[5]	-0.09(2)	M1(+E2)
633.9(1)	3814.8(3)	$31/2^- \rightarrow 27/2^-$	6.46(33)	0.96(2)[5]	0.11(4)	E2
637.8(1)	637.9(1)	$7/2^+ \rightarrow 3/2^+$	7.87(94)	1.01(2)[13]	0.04(2)	E2
642.2(1)	806.2(2)	$15/2^- \rightarrow 11/2^-$	100(6)	1.01(1)[2]	0.08(1)	E2
662.5(1)	3180.9(3)	$27/2^- \rightarrow 23/2^-$	11.69(58)	0.97(1)[5]	0.12(2)	E2
670.0(1)	2069.0(1)	$15/2^+ \rightarrow 11/2^+$	0.56(9)	0.94(5)[9]	0.11(2)	E2
671.8(1)	2866.5(3)	$25/2^+ \rightarrow 23/2^+$	1.62(8)	0.42(2)[7]	-0.03(1)	M1+E2
682.4(1)	2299.0(3)	$21/2^- \rightarrow 19/2^-$	8.61(43)	0.57(2)[5]	-0.04(1)	M1(+E2)
683.1(1)	1656.0(1)	$13/2^+ \rightarrow 9/2^+$	3.51(21)	0.99(2)[3]	0.05(2)	E2
695.2(1)	2693.9(2)	$(19/2^+) \rightarrow 15/2^+$	0.57(3)	-	-	(E2)
700.2(1)	3887.7(3)	$29/2^+ \rightarrow 27/2^+$	0.26(2)	0.51(2)[7]	-0.06(3)	M1(+E2)
700.5(1)	3792.5(3)	$27/2^- \rightarrow 25/2^-$	1.14(26)	0.69(4)[10]	-0.21(5)	M1(+E2)
704.6(1)	1045.8(2)	$13/2^- \rightarrow 9/2^-$	1.99(10)	1.89(5)[8]	0.02(1)	E2
737.2(1)	3431.1(2)	$(23/2^+) \rightarrow (19/2^+)$	0.38(8)	0.93(14)[9]	0.08(6)	E2
743.4(2)	3042.4(4)	$23/2^+ \rightarrow 21/2^-$	0.65(5)	0.47(7)[5]	-0.13(3)	M1+E2
761.0(1)	1399.1(1)	$11/2^+ \rightarrow 7/2^+$	0.97(8)	0.99(2)[9]	0.18(12)	E2
768.0(1)	2167.1(2)	$15/2^+ \rightarrow 11/2^+$	0.16(5)	1.04(4)[9]	0.05(3)	E2
780.1(1)	2436.1(2)	$17/2^+ \rightarrow 13/2^+$	1.15(26)	1.06(6)[6]	0.15(6)	E2
793.0(1)	3092.0(3)	$25/2^- \rightarrow 21/2^-$	2.26(6)	1.09(15)[2]	0.05(12)	E2
794.8(1)	1600.9(2)	$17/2^+ \rightarrow 15/2^-$	12.56(21)	0.55(1)[5]	0.03(1)	E1
810.4(1)	1616.7(2)	$19/2^- \rightarrow 15/2^-$	81(4)	1.01(1)[5]	0.10(2)	E2
815.7(1)	1861.5(3)	$17/2^{(-)} \rightarrow 13/2^-$	1.04(5)	0.92(7)[4]	0.03(6)	(E2)
833.1(1)	2489.1(2)	$17/2^+ \rightarrow 13/2^+$	0.95(21)	0.95(14)[3]	0.17(8)	E2
834.3(1)	4649.1(3)	$33/2^- \rightarrow 31/2^-$	0.21(8)	0.55(9)[5]	-0.07(5)	M1(+E2)
850.1(1)	1191.3(2)	$11/2^- \rightarrow 9/2^-$	0.20(2)	0.96(8)[8]	-0.09(5)	M1+E2
857.3(1)	1903.1(3)	$17/2^- \rightarrow 13/2^-$	0.31(2)	0.91(7)[4]	0.28(6)	E2
880.9(1)	4061.8(3)	$29/2^- \rightarrow 27/2^-$	2.69(14)	0.57(3)[5]	-0.10(3)	M1(+E2)
881.2(1)	3747.7(3)	$27/2^+ \rightarrow 25/2^+$	0.24(2)	0.54(3)[7]	-0.01(2)	M1+E2

Table I: Continued...

E_γ(Err) (in keV)	E_i(Err) (in keV)	$J_i^\pi \rightarrow J_f^\pi$	I_γ(Err) [1]	R_{DCO}(Err)	Δ_{PDCO}(Err)	Deduced Multipolarity
887.8(1)	3658.1(3)	$27/2^+ \rightarrow 23/2^+$	0.28(2)	1.01(18)[2]	0.15(10)	E2
901.6(1)	2518.4(3)	$23/2^- \rightarrow 19/2^-$	21(1)	1.01(1)[5]	0.10(1)	E2
901.8(1)	3390.9(2)	$21/2^{(+)} \rightarrow 17/2^+$	0.21(12)	0.98(17)[3]	-	(E2)
939.2(1)	4126.6(3)	$29/2^+ \rightarrow 27/2^+$	0.26(2)	0.75(7)[7]	-0.02(3)	M1+E2
942.6(1)	3192.0(3)	$23/2^+ \rightarrow 21/2^+$	1.23(10)	0.42(10)[2]	-0.15(2)	M1+E2
964.6(1)	2770.3(3)	$23/2^+ \rightarrow 19/2^+$	1.11(11)	1.01(9)[5]	0.04(3)	E2
969.8(1)	4061.8(3)	$29/2^- \rightarrow 25/2^-$	-	-	-	(E2)
978.7(1)	3585.3(3)	$29/2^{(-)} \rightarrow 25/2^{(-)}$	0.37(4)	1.04(27)[5]	0.05(15)	(E2)
979.2(1)	2025.0(3)	$15/2^{(-)} \rightarrow 13/2^-$	0.29(2)	0.62(7)[4]	-	(M1+E2)
986.2(1)	2791.8(3)	$23/2^+ \rightarrow 19/2^+$	1.43(9)	0.96(15)[5]	0.25(7)	E2
990.4(1)	3508.8(3)	$27/2^- \rightarrow 23/2^-$	2.79(23)	0.94(3)[10]	0.24(3)	E2
992.6(1)	3187.3(3)	$27/2^+ \rightarrow 23/2^+$	1.56(9)	1.04(2)[7]	0.11(1)	E2
997.2(1)	3192.0(3)	$23/2^+ \rightarrow 23/2^+$	0.08(2)	1.14(15)[7]	0.14(11)	E2
1021.3(1)	3887.7(3)	$29/2^+ \rightarrow 25/2^-$	0.34(2)	1.09(4)[7]	0.05(3)	E2
1044.5(1)	2090.3(3)	$17/2^{(-)} \rightarrow 13/2^-$	0.09(1)	0.95(13)[4]	-	(E2)
1061.8(1)	4242.7(3)	$29/2^- \rightarrow 27/2^-$	1.72(11)	0.49(4)[10]	-0.04(3)	M1+E2
1104.8(1)	3354.3(3)	$23/2^+ \rightarrow 21/2^+$	1.52(8)	1.04(15)[11]	-0.03(2)	M1(+E2)
1107.0(1)	4921.8(3)	$33/2^- \rightarrow 31/2^-$	0.27(11)	0.60(4)[10]	-0.06(3)	M1(+E2)
1130.6(1)	4945.4(3)	$35/2^- \rightarrow 31/2^-$	1.49(8)	0.94(6)[2]	0.13(3)	E2
1179.8(1)	3374.4(3)	$25/2^+ \rightarrow 23/2^+$	0.42(2)	0.49(2)[7]	-0.02(1)	M1+E2
1191.0(1)	5078.7(3)	$33/2^+ \rightarrow 29/2^+$	0.12(3)	0.96(21)[7]	0.17(12)	E2
1205.1(2)	3108.2(4)	$21/2^{(-)} \rightarrow 17/2^-$	0.26(3)	0.92(8)[4]	0.05(7)	(E2)
1276.3(1)	4463.6(3)	$31/2^+ \rightarrow 27/2^+$	-	-	-	(E2)
1561.8(1)	5376.6(3)	$35/2^- \rightarrow 31/2^-$	-	-	-	(E2)

Another sequence of levels, built on the $11/2^-$ isomer and placed parallel to the yrast band $B1$ is marked as $B5$ in the level scheme (Fig. 3). Some of the levels of this sequence were reported earlier [3]. In the present work, seven new transitions of 316, 334, 602, 857, 979, 1045 and 1205 keV have been added to this sequence extending it upto 3108 keV. The coincidence spectrum of 177 keV γ ray gate is shown in Fig. 10, in which the new transitions observed from the present work can be clearly seen. The 316 and 602 keV transitions are found to be in coincidence with the 177 keV, but not with the 705 keV and therefore placed in parallel to the 705 keV transition. Three new transitions of energies 857, 1045 and 1205 keV are found to be in coincidence with both 177 keV and 705 keV transitions and are placed above the 1046 keV level. The spin-parity of the 341 and 666 keV levels, decaying by the 177 and 502 keV transitions respectively, could not be determined from the present work and are adopted from Ref. [31]. The Δ_{PDCO} and R_{DCO} values of the 705 and 850 keV transitions could be obtained from the gate of 177 keV transition. This establishes the 705 keV and 850 keV transitions as of E2 and M1 nature respectively. The R_{DCO} values of transitions above the 1046 keV level were then determined from the quadrupole gate of 705 keV. However, due to the large uncertainty of the measured Δ_{PDCO} values of 1205 and 816 keV transitions, the parities of the corresponding levels at 3108 and 1862 keV are tentatively assigned. Whereas, the Δ_{PDCO} of 979 and 1045 keV transitions could not be measured in the present work.

The positive parity band structures, marked as $B6$ and $B6$(a) in the level scheme (Fig. 3), are developed on the $3/2^+$ ground state. In this band, few levels at lower ex-

[1] Relative γ-ray intensities are normalized to 100 for the total intensity of 642.2-keV γ-ray.
[2] From 810.4 keV E2 DCO gate;
[3] From 608.3 keV E2 DCO gate;
[4] From 704.6 keV E2 DCO gate;
[5] From 642.2 keV E2 DCO gate;
[6] From 683.1 keV E2 DCO gate;
[7] From 389.0 keV E2 DCO gate;
[8] From 177.1 keV (M1+E2) DCO gate;
[9] From 637.8 keV E2 DCO gate;
[10] From 901.6 keV E2 DCO gate;
[11] From 794.8 keV E1 DCO gate;
[12] From 1021.3 keV E2 DCO gate;
[13] From 761.0 keV E2 DCO gate;
[14] adopted from Ref. [31];

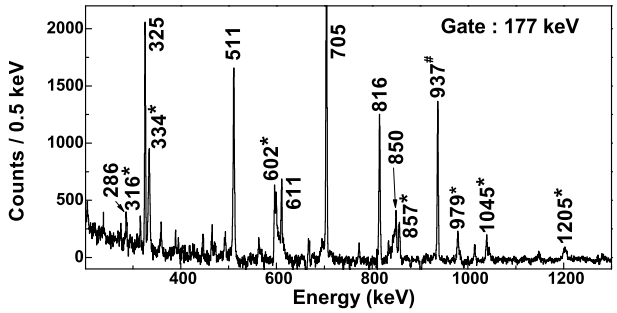

FIG. 10: Coincidence spectra corresponding to the gate of 177 keV transition of the sequence $B5$ from the E_γ-E_γ matrix. The new transitions observed in the present work are marked with $*$. γ ray marked with '#' is the contaminant γ ray coming from reactions with Mylar backing.

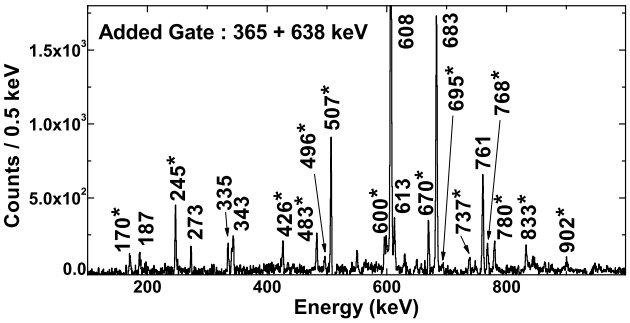

FIG. 11: Coincidence spectra corresponding to the added gates of 365 and 638 keV transitions of bands $B6$-$B6$(a), obtained from E_γ-E_γ matrix. The new transitions observed in the present work are marked with $*$.

citation upto 1999 keV having spin $15/2^+$ were reported earlier [3]. From the present measurements, this sequence has been extended upto an excitation of 3431 keV with spin $(23/2^+)$. Sixteen new transitions have been placed in the sequences named $B6$, $B6$(a), $B6$(b) $B6$(c) and $B6$(d). Fig. 11 shows the coincidence spectra corresponding to the added gates on the two lowest transitions of energies 365 and 638 keV of this sequence, where the new transitions are clearly visible. The yrast cascade of M1 and the crossover E2 transitions above the 365 keV transition are placed according to the mutual coincidence relationships and relative intensities. The connection between the 2489 keV and 1999 keV level could not be observed, probably due to very low intensity.

V. DISCUSSION

The neutron Fermi levels of the Xe isotopes with neutron number $N > 70$ lie around the $h_{11/2}$, $d_{3/2}$ and $s_{1/2}$ single particle orbitals, situated just below the $N = 82$ shell closure. The evolution of the excitation energies of the low-lying single particle configurations in Xe isotopes are shown in Fig. 12. It can be seen from this figure that the ground states of the lighter Xe isotopes are $1/2^+$ which changes to $3/2^+$ for $N = 77$ (^{131}Xe) and continues to be $3/2^+$ until $N = 81$. On the other hand, the excitation energy of the $11/2^-$ state, corresponding to the $h_{11/2}$ orbital, is minimum for the $N = 77$ (^{131}Xe) isotope. This clearly shows a transitional nature of ^{131}Xe. It is worthwhile to mention that transitional nature of the neutron number $N = 77$ accompanied by a structural change was reported for odd-odd Cs (Z = 55) isotopes [32] as well. Therefore, the neutron number $N = 77$ seems to play crucial role in determining the high spin level structure of nuclei in this $A \sim 130$ region.

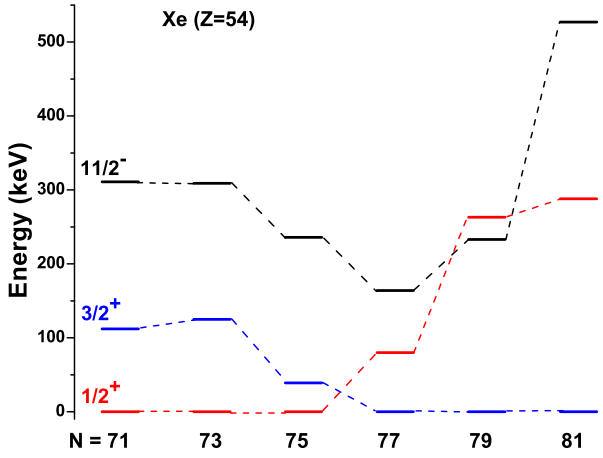

FIG. 12: Evolution of the low-lying 1-qp states in Xe isotopes.

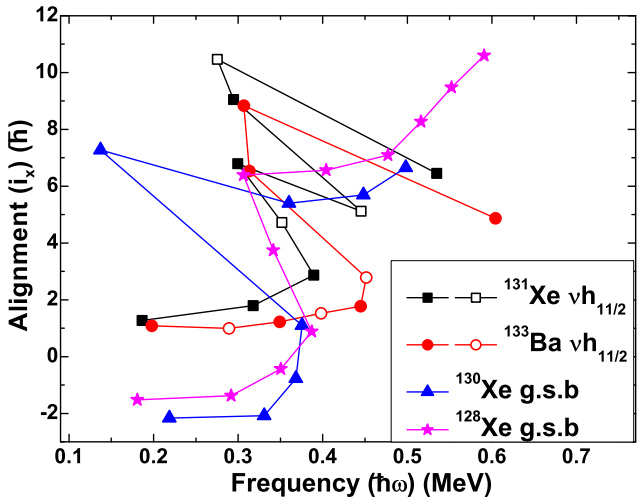

FIG. 13: Alignment plot of the $\nu h_{11/2}$ band of N = 77 isotones and the ground state band (g.s.b) of neighbouring even-even nuclei. The Harris parameters of $J_0 = 16\ \hbar^2$/MeV and $J_1 = 7\ \hbar^4$/MeV^3 were used [15]. Filled and open circles are used for two different signatures.

The band $B1$ in ^{131}Xe is a rotational band based on

$\nu h_{11/2}$ configuration. The band crossing resulted due to the alignment of a pair of protons in the $\pi h_{11/2}$ orbital was reported earlier by Kaya *et al.* [12] and was described in terms of large scale shell model calculations. It was also shown that the total aligned angular momenta (I_x) of this band show a pronounced backbending for N = 77 isotope ^{131}Xe, in contrast to the lighter odd-A Xe isotopes, suggesting again the transitional nature of the neutron number N = 77 in case of Xe isotopes while approaching the N = 82 shell closure. In order to get an idea on the single particle orbitals involved with N = 77 nuclei, the aligned single particle angular momenta (obtained by subtracting a reference angular momentum I_{ref} from the total aligned angular momentum I_x; I_{ref} is obtained from the Harris parametrization) are plotted for the $\nu h_{11/2}$ configuration of the neighbouring odd-A and even-even nuclei in Fig. 13. Both the N = 77 isotones have similar initial single particle alignments, which are about 3 $\hbar$ more than the single particle alignments of the even-even Xe core. This indicates the involvement of the $\Omega = 9/2$ component of the $h_{11/2}$ orbital i.e 9/2[514] Nilsson configuration for this band in N = 77 isotones of ^{131}Xe and ^{133}Ba. This would indicate a small or no signature splitting in this band.

However, the $11/2^-$ bands in other isotopes of Xe and in the N = 77 isotones have been observed with a reasonably large signature splitting. This cannot be accounted for in case of a large Ω configuration, like $\Omega = 9/2$, unless there is Ω mixing. The ^{129}Xe nucleus has been reported to posses triaxial shape [16], which causes the required Ω mixing and resulted in the large signature splitting. The signature partner band of the yrast $\nu h_{11/2}$ band was not known in ^{131}Xe from earlier works. In the present work, a signature partner band above $19/2^-$ state has been identified (band $B1(a)$) for the first time in this nucleus, having a large signature splitting similar to ^{129}Xe. The signature splitting can be obtained from the variation of staggering parameter, S(I), as defined by Huang *et al.* [16], as a function of 2I and are shown in Fig. 14(a) and 14(b) for ^{131}Xe along with its neighbouring isotopes and isotones respectively. The excellent agreement of the general trend and the amount of signature splitting indicate that the structure of ^{131}Xe is similar to that of its neighbours that is a triaxial or a gamma-soft shape.

Triaxial or gamma-soft shape in a nucleus gives rise to interesting structural phenomena, like wobbling motion or gamma-vibration. These phenomena are manifested in the occurrence of side bands corresponding to the multiphonon excitation of wobbling or gamma vibrations. A set of states, identified for the first time in this work as band $B1(b)$, has been observed to decay to the different states in band $B1$. These states might correspond to the excitation of gamma phonons in ^{131}Xe. But the transitions between the states in $B1$(b) could not be identified as they are of weak intensity, so it is difficult to conclude that $B1$(b) is a gamma vibrational band.

The $21/2^-$ state at 2013 keV has been observed for the first time in this work with a band like structure $B2$

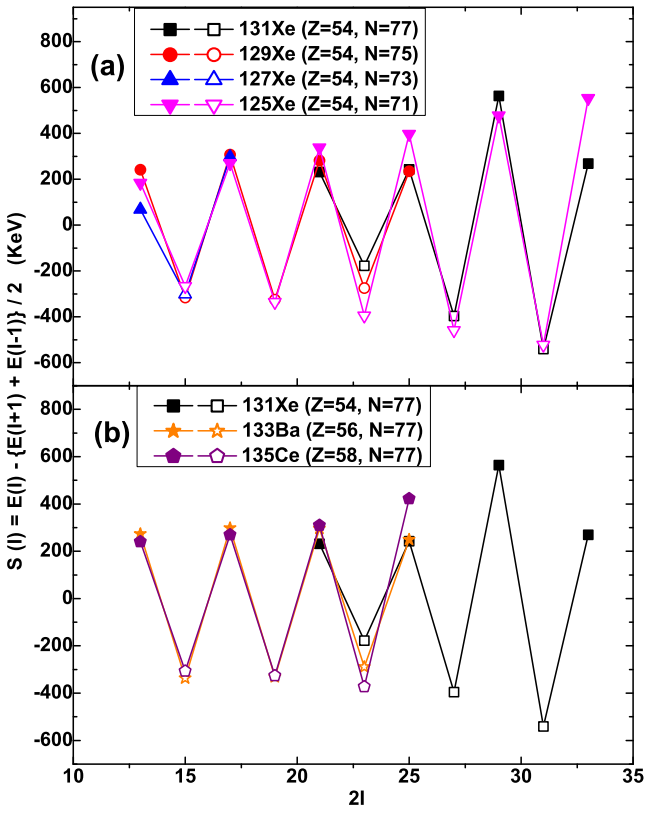

FIG. 14: Staggering of the $11/2^-$ band in ^{131}Xe are plotted as a function of spin 2I and compared with the same band of other isotopes (a) and isotones (b). Filled and open circles are used for two different signatures.

built on it. This band decays to the $19/2^-$ state of the $\nu h_{11/2}$ band $B1$. This state has not been observed in the neighbouring isotope ^{129}Xe but could be identified in the neighbouring N = 77 isotone ^{129}Te [33] at an excitation energy of 1958 keV. This state in ^{129}Te also decays to the $19/2^-$ state of the $\nu h_{11/2}$ band. Considering the similar excitation energy and decay pattern, this state has been assigned a configuration of $\pi g_{7/2}d_{5/2} \otimes \nu h_{11/2}$.

Most of the low-lying non-yrast states, which decay to the $11/2^-$ yrast isomeric state, were known from the previous work [22]. The band-like sequence $B5$ built on a $13/2^-$ state at 1046 keV has been identified in the present work. This sequence is limited up to only $21/2^{(-)}$ and seems be a decoupled band. The possible configuration of this state is the coupling of a $h_{11/2}$ neutron to the second 2^+ state of the ^{130}Xe core.

A low-lying positive parity band based on $1/2^+$ or $3/2^+$ state, as the bands $B6$ - $B6$(a) in ^{131}Xe, has been identified in the odd-A isotopes of Xe and Ba nuclei. In the lighter isotopes of these two nuclei, this band was described as a $s_{1/2}/d_{3/2}$ mixed configuration. As the neutron number increases, the occupation probability of the $d_{3/2}$ orbital increases as is evident from the lowering of

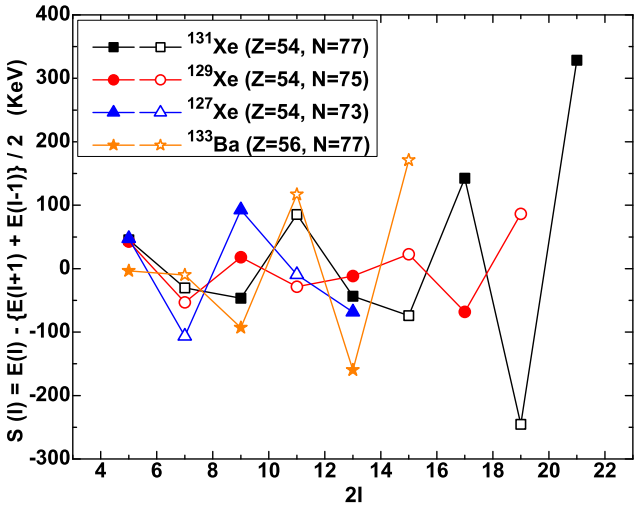

FIG. 15: The staggering, S(I), plot as a function of spin, 2I, for the low-lying positive parity bands $B6$-$B6$(a) of ^{131}Xe along with the neighbouring isotopes and isotone. Filled and open circles are used for two different signatures.

the excitation energy of the $3/2^+$ state with the increase in neutron number in both Ba and Xe nuclei. In case of ^{133}Ba, the $N = 77$ isotone of ^{131}Xe, the excitation energies of the $3/2^+$ and the $1/2^+$ states are very close to each other (within about 12 keV) and hence, this band in ^{133}Ba was identified with a $d_{3/2}$ configuration [2]. In ^{131}Xe, the $3/2^+$ state is the ground state and the $1/2^+$ state is about 80 keV above it (Fig. 12), indicating a more pure $d_{3/2}$ configuration for the bands $B6$-$B6$(a) in ^{131}Xe. It is also interesting to note that for the nuclei in the $N = 77$ isotonic chain, the relative positions of the $1/2^+$ and the $3/2^+$ states alter at $Z = 54$, while approaching down to $Z = 50$. The $3/2^+$ state becomes lower in energy for the $Z = 54$ nucleus ^{131}Xe. Therefore, both in isotopic and in isotonic chains, ^{131}Xe behaves as a transitional nucleus.

In the present work, both the signature partners of the bands $B6$ and $B6$(a) are well established and extended up to $23/2\ \hbar$ and so the signature splitting or the staggering parameter S(I), of these bands can also be compared with the other isotopes and isotones as shown in Fig. 15. It can be seen that the staggering in the Xe isotopes decreases with increasing neutron number indicating less contribution from low-Ω orbitals for the heavier isotopes. On the other hand, the S(I) values for the $N = 77$ isotones, ^{131}Xe and ^{133}Ba are very similar. A signature inversion at $I = 15/2\ \hbar$ has been observed in ^{131}Xe, similar to that of ^{129}Xe, but the phases are opposite. Data for the $N = 77$ isotones are not available to observe any inversion around that spin. It can be seen that after the inversion, the splitting increases rapidly for ^{131}Xe, indicating a change in shape to an oblate or a triaxial deformation.

A few sequences of states ($B6$(b), $B6$(c) and $B6$(d)) in Fig. 3 have been observed to decay to the band $B6$ and $B6$(a). As these states decay to the positive parity ground state band with neutron $d_{3/2}$ configuration, therefore, the most likely configuration of the $13/2^+$ state at 1586 keV would be $\pi g^2_{7/2} \otimes \nu d_{3/2}/s_{1/2}$.

The $17/2^+$ and the $19/2^+$ states at 1.6 and 1.8 MeV excitation energies in the lower part of band $B4$, decays strongly to the $11/2^-$ (band $B1$) band. This indicates that these states have same $\nu h_{11/2}$ configuration. The excitation energies of these states suggest that they are of three quasiparticle in nature. In ^{129}Xe, a three quasiparticle $19/2^+$ state at 2.2 MeV was assigned a proton configuration of $\pi(g_{7/2} \otimes h_{11/2})$ coupled with a low-Ω neutron at $1/2^-[541]$ Nilsson orbital to interpret the rotational band structure with large signature splitting observed on top of that state [16]. In ^{131}Xe, the $17/2^+$ and the $19/2^+$ states are also assigned a similar generic configuration of $\pi g_{7/2}h_{11/2} \otimes \nu h_{11/2}$. However, these states do not seem to form a rotational structure. Therefore, unlike ^{129}Xe, the configuration of these states does not seem to contain any deformation driving low-Ω Nilsson component. This is consistent with the conclusion of the involvement of high-Ω Nilsson orbitals in regard to the discussion of band $B1$.

The upper part of the band $B3$ (from $23/2^+$) is connected with its lower part through a high energy (1105 keV) transition. This indicates a 5-qp configuration for the upper part of this band. These states do not decay to the upper part of the band $B1$ which has the configuration of $\pi h^2_{11/2} \otimes \nu h_{11/2}$. Therefore, two proton $h_{11/2}$ configuration may be excluded for this part of band $B3$. Considering their positive parity, the $23/2^+$ and the $25/2^+$ states are likely to be formed by the alignment of an additional pair of protons in the $g_{7/2}/d_{5/2}$ orbital with the 3-qp configuration of the lower part of this band. In the neighbouring even-even nucleus, ^{130}Xe, there is a 5^+ state at about 2.4 MeV of excitation energy, which has been assigned a two quasi-proton configuration of $\pi d_{5/2}g_{7/2}$ [34, 35]. The $27/2^+$ state in band $B3$ of ^{131}Xe might have formed by the coupling of this 5^+ state with the 3-qp configuration of the $17/2^+$ state in the lower part of band $B3$. Therefore, a configuration of $\pi(d_{5/2}g_{7/2})^3 h_{11/2} \otimes \nu h_{11/2}$ can be assigned to the upper part of the band $B3$.

A lower lying $23/2^+$ state at an excitation energy of about 2.2 MeV was known earlier in ^{131}Xe [12]. The band structures, $B4$-$B4$(a), have been identified on top of this state in the present work, with a large signature splitting. This band decays to the $19/2^+$ state at 1.8 MeV. This band is analogous to the 3-qp decoupled band in ^{129}Xe involving a deformation driving low-Ω orbital. Therefore, bands $B4$ and $B4$(a) in ^{131}Xe have been assigned a configuration of $\pi(g_{7/2}h_{11/2}) \otimes \nu f_{7/2}$. In this configuration, the $[541]1/2^-$ component of the neutron $f_{7/2}$ orbital provides the required large Coriolis force which generates the large signature splitting, as shown in Fig. 16. As it has been pointed out in the discussion of band $B1$, a large signature splitting may also corresponds to a triaxial shape.

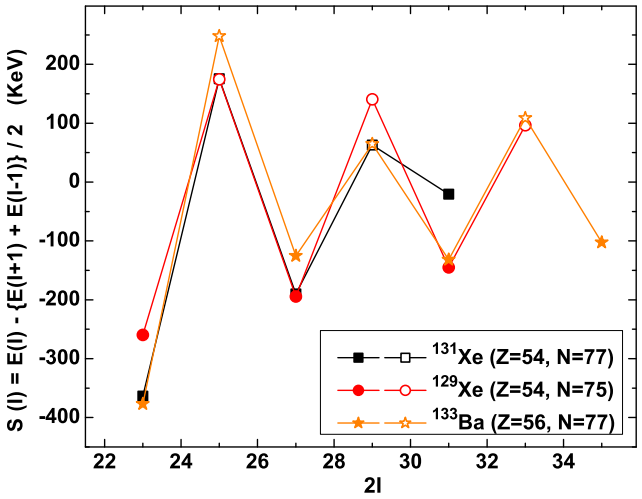

FIG. 16: The staggering, S(I), plot as a function of spin, 2I, for the bands $B4$ and $B4$(a) of ^{131}Xe alongwith the similar bands in the neighbouring isotope and isotone. Filled and open circles are used for two different signatures.

So, a non-axial deformation or gamma-softness of ^{131}Xe again in the configuration of bands $B4$-$B4$(a) is expected. For a gamma-soft shape, a gamma band is also expected. A gamma band forms a side band of the main band and decays to the main band. It is interesting that another set of states, $23/2^+$, $25/2^+$, $29/2^+$, $33/2^+$, has been identified (named as band $B4$(b)) in the present work, which forms a side band to $B4$ and decays to it. This side band may constitute the expected gamma band of $B4$. However, transitions between the states of this side band could not be identified and hence, the ratio of inter to intra band transition probabilities could not be obtained to get a conclusive evidence.

Various configurations assigned to the different band structures observed in the present work are tabulated in Table II.

TABLE II: Configuration assignments to the various bands observed in ^{131}Xe from the present work.

Band No.	Parity	Assigned configuration
Band 1	Negative	$(0^+)_{^{130}Xe} \otimes \nu h_{11/2}$
Band 2	Negative	$\pi g^2_{7/2} \otimes \nu h_{11/2}$
Band 3	Positive	$\pi(g_{7/2}d_{5/2})^3 h_{11/2} \otimes \nu h_{11/2}$
Band 4	Positive	$\pi(g_{7/2}h_{11/2}) \otimes \nu f_{7/2}$
Band 5	Negative	$(2^+_2)_{^{130}Xe} \otimes \nu h_{11/2}$
Band 6	Positive	$\nu d_{3/2}$

VI. TOTAL ROUTHIAN SURFACE (TRS) CALCULATION

In order to understand the structure of ^{131}Xe for different configurations, total Routhian surface (TRS) calculations have been performed using Strutinski shell correction method. The formalism of Nazarewicz *et al.* [36, 37] has been used with a Woods-Saxon potential to calculate the single particle energies. The procedure as depicted in Ref.[38] has been followed. The TRSs are calculated in the $\beta_2-\gamma$ deformation mesh points with minimization on β_4. The Lund convention, in which $\gamma = 0°$ (-60°) corresponds to prolate (oblate) shape, has been followed to define the nuclear shape. The surfaces are calculated for different rotational frequencies ($\hbar\omega$). The values of β_2 and γ, for which the minimum of TRS is obtained, has been used to determine the shape of the nucleus.

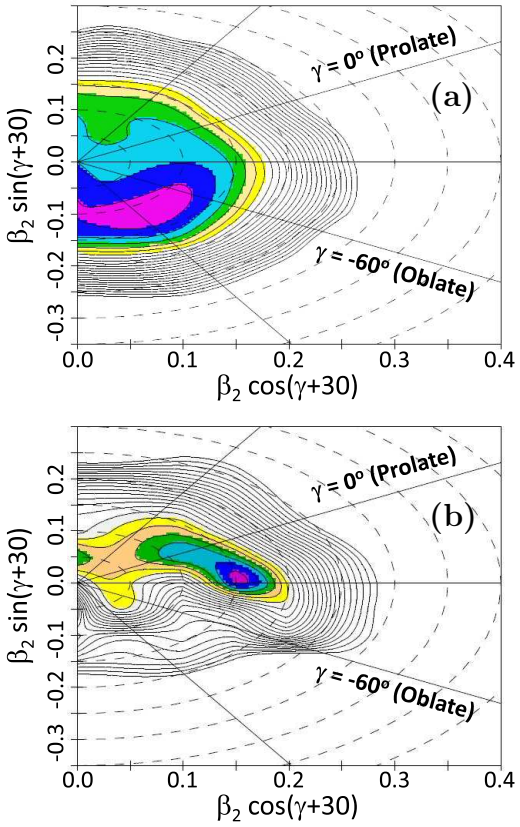

FIG. 17: Contour plots of total Routhian surfaces in the $\beta_2-\gamma$ deformation mesh calculated for the lowest negative parity configuration corresponding to the $\nu h_{11/2}$ band (band $B1$) in ^{131}Xe at the rotational frequencies ($\hbar\omega$) = 0.11 MeV (a) and 0.26 MeV (b).

The TRSs for the lowest negative parity configuration, corresponding to the $h_{11/2}$ band (band $B1$ in the level scheme of Fig. 3) are shown in Fig. 17(a) and 17(b) for two different rotational frequencies of $\hbar\omega$ = 0.11 and 0.26 MeV, respectively. It can be seen that the minimum at lower rotational frequency is spread over a region of γ around $\gamma \sim -75°$ that is, the nucleus displays γ-softness close to the ground state. However, at a slightly higher frequency of $\hbar\omega \sim 0.26$ MeV (Fig. 17(b)), a triaxial shape emerges. This frequency corresponds to the lower part of the band $B1$. This prediction of triaxial shape for the $\nu h_{11/2}$ band in ^{131}Xe is in line with that of its neigh-

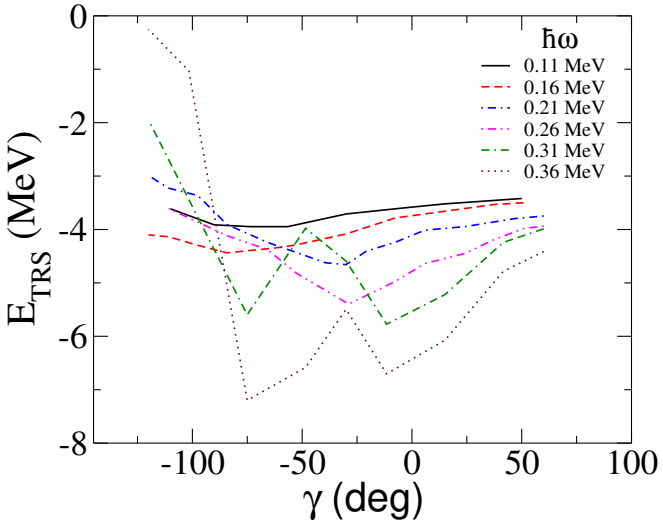

FIG. 18: Plot of total Routhian surface energies (E_{TRS}) as a function of the deformation parameter, γ calculated for the 1-qp, negative parity configuration corresponding to the $\nu h_{11/2}$ band in ^{131}Xe at different values of rotational frequencies ($\hbar\omega$)

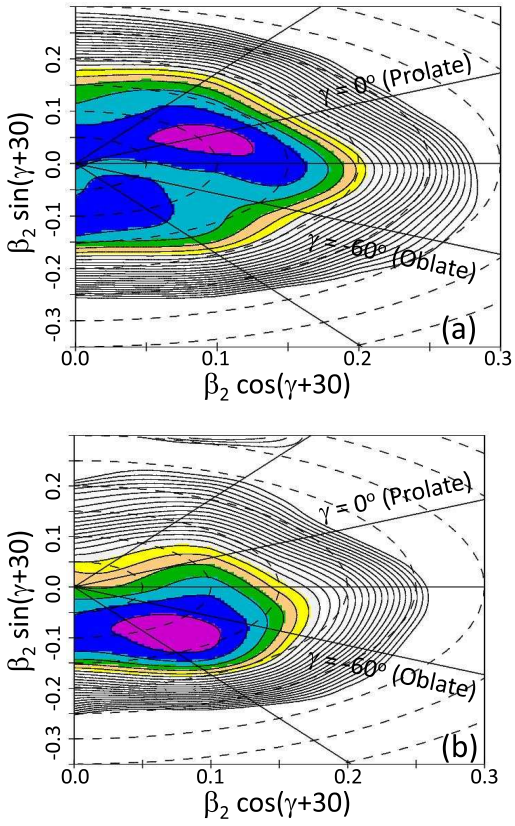

FIG. 19: Same as Figure 17 but for the lowest positive parity configuration, corresponding to the $\nu d_{3/2}$ band (bands $B6$-$B6$(a)) in ^{131}Xe at rotational frequencies ($\hbar\omega$) = 0.16 MeV (a) and 0.36 MeV (b).

bouring isotope ^{129}Xe [16] with very similar value of the

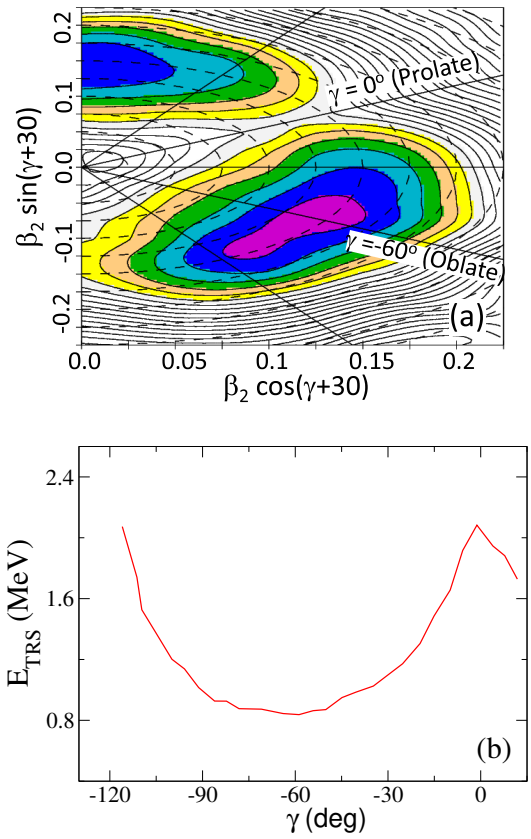

FIG. 20: (a) Same as Figure 17 but for the 3-qp configuration, corresponding to the bands $B4$-$B4$(a) in ^{131}Xe. (b) The TRS energies as a function of the deformation parameter γ for β_2 value around the minimum of the TRS.

triaxial parameter $\gamma \sim -26°$.

Variation of the calculated total Routhian energies (E_{TRS}) as a function of the deformation parameter γ is shown in Fig.18 for the negative parity $h_{11/2}$ band in ^{131}Xe. These are plotted for different rotational frequencies, $\hbar\omega$. Values of the deformation parameter β_2 were fixed around which the minimum of the TRS was obtained for each $\hbar\omega$. It can be seen that there are three distinct regions of gamma values corresponding to minimum of TRS. At low rotational frequencies ($\hbar\omega$ = 0.11 and 0.16 MeV), E_{TRS} shows some extent of γ-softness. At mid frequencies ($\hbar\omega$ = 0.21 and 0.26 MeV), the minima shift to a triaxial deformation with $\gamma \sim -26°$. At even higher frequencies ($\hbar\omega$ = 0.31 and 0.36 MeV), two minima appear at $\gamma \sim -12°$ and $\gamma \sim -75°$. This gives an interesting structural evolution, from gamma-softness to triaxial shape coexistence, with rotational frequency of the $h_{11/2}$ band in the transitional nucleus ^{131}Xe.

The TRS plots for the positive parity $\nu d_{3/2}$ configuration corresponding to the bands $B6$ and $B6$(a) in ^{131}Xe are shown in Fig. 19 for the two rotational frequencies, $\hbar\omega$ = 0.16 MeV and 0.36 MeV. It can be seen that the calculations predict a near prolate shape at lower rotational frequency which changes to a triaxial shape with

near oblate deformation at higher rotational frequency. This corroborates well with the observed increase in the staggering at higher spins for this band after the signature inversion (see Fig. 15).

The TRSs for the 3-qp configuration corresponding to the bands $B4$ and $B4$(a) are shown in Fig. 20(a). It shows minimum at about an oblate deformation with $\beta_2 \sim 0.15$ and $\gamma \sim -60^\circ$ and a large extent of gamma-softness. In Fig. 20(b), the variation of the TRS energy (E_{TRS}) around the minimum for this surface has been plotted as a function of the deformation parameter γ. The gamma-softness can be clearly seen in this plot. The minimum value of E_{TRS} remains within 100 keV for the variation of γ in the range $-86^\circ \leq \gamma \leq -45^\circ$. The observed large staggering and a possible gamma-band associated with the bands $B4$-$B4$(a) in ^{131}Xe is in good agreement with the above prediction of oblate minimum with gamma-softness.

VII. SUMMARY

The excited states in ^{131}Xe have been investigated by populating them using the fusion evaporation reaction ^{130}Te(α, $3n$)^{131}Xe at 38 MeV of beam energy. The INGA detector setup at VECC, Kolkata, was used to detect the γ-rays. A much improved and extended level scheme with several new band structures has been obtained with the observation of 72 new γ transitions in this work. Different variety of yrast and non-yrast band structures have been observed in this nucleus by using α-induced reaction. The identification of these bands, based on different quasi-particle configurations, reveals the existence of different structures in the $N = 77$ transitional nucleus ^{131}Xe. The new data on the signature splitting and the single particle alignment of the lowest negative parity band ($B1$), having $\nu h_{11/2}$ character, indicate a triaxial shape with the involvement of a high-Ω Nilsson orbital. The lowest positive parity band ($B6$-$B6$(a)) has been substantially extended. This band shows signature inversion at moderate spin, which, along with a large signature splitting after the inversion, indicates a change in structure at higher spins. Two new band structures, a 3-qp band having configuration $\pi(g_{7/2}h_{11/2}) \otimes \nu f_{7/2}$ ($B4$) with large staggering and a 5-qp dipole band having configuration $\pi(g_{7/2}d_{5/2})^3 h_{11/2} \otimes \nu h_{11/2}$ ($B3$) have been identified. The configurations of different bands have been assigned from the systematics of neighbouring odd-A and even-even nuclei and considering the available orbitals near the proton and the neutron Fermi levels. Theoretical TRS calculations for the 1-qp and 3-qp band configurations suggest interesting structural evolution which corroborates well with the experimental findings. Triaxial shape and gamma-softness are obtained for the 3-qp configurations. New sets of states have been identified which have been found to decay to these 3-qp, negative and positive parity bands. This gives interesting prospects of the observation of gamma-bands associated with these 3-qp configurations, which needs to be further investigated.

VIII. ACKNOWLEDGMENTS

The authors would like to thank all the INGA collaborators, for setting up the INGA at VECC, Kolkata. The authors also acknowledge the staffs of the Accelerator group at VECC for providing good quality α beam for the present experiment. The support of CEFIPRA/IFCPAR for the present work under Project No. 5604-4 is thankfully acknowledged. The authors would also like to thank A. Navin for his support and encouragement for the present work. R. B and S. N acknowledge with thanks the financial support received as research fellows from the Department of Atomic Energy (DAE), Government of India. S. R. would like to acknowledge the financial assistance from the University Grants Commission Minor Research Project [Project No. PSW-249/15-16 (ERO)] and the FRPDF grant of Presidency University, Kolkata, India. H. P. is grateful for the support of the Ramanujan Fellowship research grant under SERB-DST (SB/S2/RJN-031/2016). P. R acknowledges University Grant Commission for her fellowship (Sr. No. 2121551170 and Ref. No. 20/12/2015(ii)EU-V). INGA is partially funded by Department of Science and Technology, Government of India, vide INGA project No. IR/S2/PF-03/2003-I.

[1] R. Wyss, A. Granderath, R. Bengtsson, P. Von Brentano, A. Dewald, A. Gelberg, A. Gizon, J. Gizon, S. Harissopulos, A. Johnson, W. Lieberz, W. Nazarewicz, J. Nyberg and K. Schiffer, Nucl. Phys. A **505**, 337 (1989).

[2] S. Juutinen, P. Simecek, P. Ahonen, M. Carpenter, C. Fahlander, J. Gascon, R. Julin, A. Lampinen, T. Lönnroth, J. Nyberg, A. Pakkanen, M. Piiparinen, K. Schiffer, G. Sletten, S. Törmänen and A. Virtanen, Phys. Rev. C **51**, 1699 (1995).

[3] T. Lönnroth, J. Kumpulainen and C. Tuokko, Physica Scripta. **27**, 228, (1983).

[4] N.V. Zamfir and R.F. Casten, Phys. Lett. B **260**, 265 (1991).

[5] A.P. Byrne, K. Schiffer, G.D. Dracoulis, B. Fabricius, T. Kibédi, A.E. Stuchbery and K.P. Lieb, Nucl. Phys. A **548**, 131 (1992).

[6] R. Ma, E.S. Paul, D.B. Fossan, Y. Liang, N. Xu, R. Wadsworth, I. Jenkins and P.J. Nolan, Phys. Rev. C, **41**, 2624 (1990).

[7] A. Granderath, P.E. Mantica, R. Bengtsson, R. Wyss, P. von Brentano, A. Gelberg, E Seiffert, Nucl. Phys. A **597**, 427 (1996).

[8] R.F. Casten and P. von Brentano, Phys. Lett. B **152**, 22 (1985).

[9] K. Nomura, T. Niksic and D. Vretenar, Phys. Rev. C **96**, 014304 (2017).

[10] E. Teruya, N. Yoshinaga, K. Higashiyama and A. Odahara, Phys. Rev. C, **92**, 034320 (2015).

[11] A. Astier, M.-G. Porquet, Ts. Venkova, Ch. Theisen, G. Duchêne, F. Azaiez, G. Barreau, D. Curien, I. Deloncle, O. Dorvaux, B.J.P. Gall, M. Houry, R. Lucas, N. Redon, M. Rousseau and O. Stézowski, Eur. Phys. J. A **50**, 2 (2014).

[12] L. Kaya *et al.*, Phys. Rev. C **98**, 014309 (2018).

[13] A. Al-Khatib, G.B. Hagemann, G. Sletten, A.K. Singh, H. Amro, G. Benzoni, A. Bracco, P. Bringel, F. Camera, M.P. Carpenter, P. Chowdhury, R.M. Clark, C. Engelhardt, P. Fallon, B. Herskind, H. Hübel, R.V.F. Janssens, T.L. Khoo, T. Lauritsen, A. Neuber-Neffgen and C. Ronn Hansen, Phys. Rev. C **83**, 024306 (2011).

[14] S. Chakraborty, H.P. Sharma, S.S. Tiwary, C. Majumder, P. Banerjee, S. Ganguly, S. Rai, Pragati, Swati Modi, P. Arumugam, Mayank, S. Kumar, R. Palit, A. Kumar, S.S. Bhattacharjee, R.P. Singh, and S. Muralithar, Phys. Rev. C **97**, 054311 (2018).

[15] S. Chakraborty, H.P. Sharma, S.S. Tiwary, C. Majumder, P.K. Prajapati,S. Rai, P. Popli, M. Singh, S.S. Bhattacharjee, R.P. Singh, S. Muralithar, P. Banerjee, S. Ganguly, S. Kumar, A. Kumar and R. Palit, Braz. Jour. of Phys. **47**, 406 (2017).

[16] Y. Huang, Z.G. Xiao, S.J. Zhu, C. Qi, Q. Xu, W. J. Cheng, H.J. Li, L.M. Lyu, R.S. Wang, W.H. Yan, H. Yi, Y. Zhang, Q.M. Chen, C.Y. He, S.P. Hu, C.B. Li, H.W. Li, P.W. Luo, X.G. Wu, Y.H. Wu, Y. Zheng and J. Zhong, Phys. Rev. C **93**, 064315 (2016).

[17] G. Rainovski, D.L. Balabanski, G. Roussev, G. Lo Bianco, G. Falconi, N. Blasi, D. Bazzacco, G. de Angelis, D.R. Napoli, F. Dönau and V.I. Dimitrov, Phys. Rev. C **66**, 014308 (2002).

[18] R.A. Meyer, F. Momyer and W. B. Walters, Z. Physik **268**, 387 (1974).

[19] A.D. Irving, P.D. Forsyth, I. Hall and D.G.E Martin, J. Phys. G: Nucl. Phys. **5**, 1595 (1979).

[20] D.C. Palmer, A.D. Irving, P.D. Forsyth, I. Hall, D.G.E. Martin and M.J Maynard, J. Phys. G: Nucl. Phys. **4**, 1143 (1978).

[21] Chr. Bargholtz, S. Beshai and L. Gidefeldt, Nucl. Phys. A **270**, 189 (1976).

[22] A. Kerek, A. Luukko, M. Grecescu and J. Sztarkier, Nucl. Phys A **172**, 603 (1971).

[23] Soumik Bhattacharya, R. Banik, S. Nandi, Sajad Ali, S. Chatterjee, S. Das, S. Samanta, K. Basu, A. Choudhury, A. Adhikari, S.S. Alam, Shabir Dar, B. Das, Sangeeta Das, A. Dhal, A. Mondal, K. Mondal, P. Mukhopadhyay, H. Pai, P. Ray, A. Saha, I. Shaik, C. Bhattacharya, G. Mukherjee, R. Raut, S.S. Ghugre, A. Goswamiand S. Bhattacharyya, Proceedings of the DAE Symp. on Nucl. Phys. **63**, 1156 (2018).

[24] S. Das, S. Samanta, R. Banik, R. Bhattacharjee, K. Basu, R. Raut, S.S. Ghugre, A.K. Sinha, S. Bhattacharya, S. Imran, G. Mukherjee, S. Bhattacharyya, A. Goswami, R. Palit, H. Tan, Nucl. Instrum. and Methods in Phys. Res. A, 893, 138 (2018).

[25] D. C. Radford, Nucl. Instrum. Methods Phys. Res. A, 361, 297 (1995).

[26] http://www.tifr.res.in/ pell/lamps.html

[27] A. Krämer-Flecken, T. Morek, R.M. Lieder, W. Gast, G. Hebbinghaus, H.M. Jäger and W. Urban, Nucl. Instrum. Methods Phys. Res. A **275**, 333 (1989).

[28] K. Starosta, T. Morek, Ch. Droste, S.G. Rohoziński, J. Srebrny, A. Wierzchucka,M. Bergström, B. Herskind, E. Melby, T. Czosnyka, P.J. Napiorkowski, Nucl. Instrum. Methods Phys. Res. A **423**, 16 (1999).

[29] Ch. Droste, S.G. Rohoziński, K. Starosta, T. Morek, J. Srebrny and P. Magierskib, Nucl. Instrum. Methods Phys. Res. A **378**, 518 (1996).

[30] https://www-nds.iaea.org/public/ensdf_pgm/.

[31] Yu. Khazov, I. Mitropolsky, A. Rodionov, Nucl. Data Sheet **107**, 2715 (2006).

[32] H. Pai, G. Mukherjee, A. Raghav, R. Palit, C. Bhattacharya, S. Chanda, T. Bhattacharjee, S. Bhattacharyya, S.K. Basu, A. Goswami, P. K. Joshi, B. S. Naidu, Sushil K. Sharma, A.Y. Deo, Z. Naik, R.K. Bhowmik, S. Muralithar, R.P. Singh, S. Kumar, S. Sihotra and D. Mehta, Phys. Rev. C **84**, 041301(R) (2011).

[33] C.T. Zhang, P. Bhattacharyya, P.J. Daly, Z.W. Grabowski, R.H. Mayer, M. Sferrazza, R. Broda, B. Fornal, W. Królas, T. Pawlat, D. Bazzacco, S. Lunardi, C. Rossi Alvarez and G. de Angelis, Nucl. Phys. **A628**, 386 (1998).

[34] L. Goettig, Ch. Droste, A. Dygo, T. Morek, J. Srebrny, R. Broda, J. Styczeń, J. Hattula, H. Helppi and M. Jääskeläinen, Nucl. Phys. **A 357**, 109 (1981).

[35] T. Lönnroth, J. Haitula, H. Helppi, S. Juutinen and K. Honkanen, Nucl. Phys. **A431**, 256 (1984).

[36] W. Nazarewicz, J. Dudek, R. Bengtsson, T. Bengtsson and I. Ragnarsson, Nucl. Phys. **A 435**, 397 (1985).

[37] W. Nazarewicz, M.A. Riley and J.D. Garrett, Nucl. Phys. **A 512**, 61 (1990).

[38] G. Mukherjee, P. Joshi, R.K. Bhowmik, S.N. Roy, S. Dutta, S. Muralithar and R.P. Singh, Nucl. Phys. **A 829**, 137 (2009).